Metrology-grade spectroscopy source based on an optical parametric oscillator

Magnus Schenkel, Victor Vogt, Stephan Schiller

Research Article | Vol. 32, No. 24 / 18 Nov 2024 / Optics Express 43350

Optics EXPRESS

Metrology-grade spectroscopy source based on an optical parametric oscillator

M. R. Schenkel,[1,2] V. A. Vogt,[1] and S. Schiller[1,3]

[1] Heinrich-Heine-Universität Düsseldorf, Mathematisch-Naturwissenschaftliche Fakultät, Institut für Experimentalphysik, 40225 Düsseldorf, Germany
[2] magnus.schenkel@hhu.de
[3] step.schiller@hhu.de

Abstract: Continuous-wave optical parametric oscillators (OPOs) are widely tunable and powerful sources of narrow-linewidth radiation. These properties make them suitable for a wide range of spectroscopic studies - but so far not at the metrological level. Indeed, although important technical OPO developments occurred more than two decades ago, and commercial devices have been available for nearly as long, the long-hoped-for the potential of these devices, providing simultaneously ultralow linewidth, ultrahigh frequency stability, ultrahigh frequency accuracy, and wide wavelength coverage has not yet become a reality. Here, we present an OPO metrology system suitable for optical spectroscopy with ultra-high resolution and accuracy in the 2.2 - 3.9 μm range. The system relies on the second-harmonic generation of the idler wave to bridge the gap to the near-infrared regime where frequency combs are readily available. By actively controlling the pump laser frequency, the idler radiation is phase-locked to an optically stabilized frequency comb, enabling a full transfer of the frequency comb's spectral properties to the idler radiation and measuring the idler frequency with ultra-high precision. We reach fractional line widths and Allan deviations of the idler radiation at the level of 4×10^{-14} and 1×10^{-14}, respectively. We also perform a thorough characterization of the stabilized OPO via a comparison with a second, independent optically stabilized frequency comb and thereby determine an overall idler frequency systematic uncertainty of less than 1.2×10^{-14}. Sources of residual frequency noise are identified. The system delivered excellent results in high-accuracy spectroscopy.

1. Introduction

High-resolution laser spectroscopy of atoms and molecules is a key branch of physics and physical chemistry. The spectroscopic study of many species can be performed with semiconductor lasers emitting in the near-infrared (NIR) spectral range and even in the visible range. But these sources do not satisfy all needs. An important area of laser spectroscopy is rovibrational spectroscopy, where one often wishes to measure a large set of transitions of a given molecular species, or of several different species, hence requiring a wide tuning range. The mid-infrared (MIR) range provides the most important window on rovibrational spectra. In this range, continuous-wave (cw) optical parametric oscillators (OPOs) are a unique type of spectroscopy source; their output can cover more than an octave in frequency, and the output power can be 1 W or higher. The combination of these properties sets them apart from other important MIR sources, such as DFB and quantum cascade lasers or difference-frequency generation.

Key developments in the design and performance of cw OPO devices and spectroscopy demonstrations, occurred more than two decades ago, with the first demonstrations of mode-hop-free oscillation [1–8]. Soon, the first commercial OPO devices became available. Since then, many groups have successfully used cw OPOs for diverse applications in molecular spectroscopy

#538442 https://doi.org/10.1364/OE.538442
Journal © 2024 Received 2 Aug 2024; revised 13 Sep 2024; accepted 15 Sep 2024; published 13 Nov 2024

Optics EXPRESS

[9–21], and in some instances atomic spectroscopy [22]. Only in the past decade has there been a greater need to achieve ultra-high resolution and corresponding frequency accuracy with OPOs. Metrology-grade OPOs would be useful, for example, in fundamental physics to probe the hyperfine transition of highly charged ions [23], the rovibrational transitions of simple (few-electron) molecules (such as the molecular hydrogen ions [24,25], the neutral hydrogen molecules [26–31], and the helium hydride ions ([32,33] and references therein)), or to search for a time-drift of molecular vibrational frequencies [34–37].

The wide tuning range of cw OPOs immediately raises the question of how to precisely determine the actual emission frequency. With the invention of the optical frequency comb (OFC) [38,39], a new tool emerged for measuring optical frequencies with an accuracy improved by many orders of magnitude compared to previous means. Already early studies explored how to combine an OPO with an OFC in order to enable OPO output frequency determination. Importantly, an OFC also offers the possibility to serve as a reference for stabilizing the OPO frequency by feedback control [40]. The latter option is superior to locking the frequency to molecular absorption lines because they do not offer a continuous wavelength coverage. An additional benefit would be a link of the visible and NIR regimes with the MIR regime [41]. These early demonstrations have been followed by further studies, and Table 1 presents a selection of those performed over the past decade and aimed at metrology. It is evident that it has not yet been possible to imbue an OPO with the four key properties of a metrology-grade spectroscopy source: ultralow linewidth, ultrahigh frequency stability, ultrahigh frequency accuracy, and wide wavelength coverage. The contrast with what has been achieved with diode lasers is striking: the first three properties are achieved in many metrological studies (mostly for atomic spectroscopy, e.g. for optical atomic clocks [42,43]). Clearly, there appears to be an unrealized potential for OPOs, i.e. the opportunity for developing methods capable of pushing both the linewidth and the long-term frequency instability down to the Hertz level.

Table 1. Comparison of some features of the present source in comparison to selected published works of other groups. The acronyms are defined in the text. τ is the integration time.

Ref.	Technique	Idler range (μm)	Frequency stability of idler radiation		Idler output power
			Short-term (linewidth)	Long-term (Allan deviation or other)	
Ricciardi et al. [14]	Frequency lock of pump and signal to NIR OFC	[2.7, 4.2]	$\leq$ 200 kHz at 100 ms	$\sigma_y \leq 3\times10^{-12}/\sqrt{\tau}$ for $\tau \in [1, 200]$ s	>1 W
Peltola et al. [44]	Frequency lock of idler's SH to NIR OFC	[2.7, 3.4]	$\simeq$ 1 MHz	$\sigma_y \in [10, 200]$ kHz for $\tau<10$ s	>0.5 W
Ricciardi et al. [45]	Direct cavity stabilization	[2.7, 4.2]	920 Hz at 100 ms	not stated	$\simeq$ 0.5 W
Karhu et al. [46]	OPO locked to a MIR OFC	[2.5, 4.4]	0.5 MHz at 0.15 s, 1.5 MHz at 1 s	Standard deviation of 90 kHz over 20 min	up to 0.8 W
Zhang et al. [20]	Pump locked to NIR OFC, OPO cavity locked to ULE resonator	[2.6, 4.3]	<20 kHz at 1 − 5 s	$\sigma_y<1$ kHz for $\tau>1$ s	$\simeq$ 0.4 W
This work	PLL of idler's SH to NIR OFC	[2.2, 3.9]	$\leq$ 5 Hz at $1-10^3$ s	$\sigma_y \leq 3$ Hz for $\tau>1$ s	>1 W

Optics EXPRESS

Here we present a general and effective method of OPO frequency stabilization that is fairly independent of the desired output wavelength. By locking the OPO's idler frequency to an OFC, we simultaneously achieve all four of the key properties above, improving these parameters by a combined factor of more than 10^4. We thereby demonstrate a MIR spectroscopy source with a fractional frequency instability $\leq 1 \times 10^{-14}$ on timescales between 1 and 10^5 s, an idler linewidth on the order of a few Hertz, and an SI-traceable frequency. Our frequency stabilization scheme can be operated at different idler wavelengths. This demonstrates that the method is wavelength-independent.

1.1. Frequency stabilization approaches

Since the frequency conversion process in an OPO must satisfy energy conservation at the photon level, the frequencies ω_p, ω_s and ω_i of pump, signal and idler waves, respectively, are related by

$$\omega_p = \omega_s + \omega_i \,. \tag{1}$$

If the idler wave is the main interest for a spectroscopic application, two different approaches to stabilize its frequency ω_i may be distinguished.

Consider first the approach where both ω_p and ω_s are actively stabilized, so that according to Eq. (1) the idler frequency is also stabilized. To do so, both the pump and the signal wave frequencies must be stabilized separately. Both these frequencies usually fall into the NIR range (e.g. $\lambda_p = 1.06\,\mu$m and $\lambda_s \in [1.45\,\mu\text{m}, 2.07\,\mu\text{m}]$ in this work), where narrow-linewidth and ultra-stable optical frequency combs (OFCs) can be realized with relative routine. These two properties can be achieved by phase-locking the OFC to a reference laser, which is itself frequency-locked to an ultra-stable reference cavity.

The frequency of the pump wave can be stabilized to such a comb. It is more difficult to do so for the signal wave because its frequency is determined by the resonance of the OPO cavity. One needs the ability to control the optical path length of the cavity with high bandwidth. This is challenging in view of the typical design of the OPO cavity and the cavity length actuator. The task could be eased by employing either an OPO cavity that exhibits good passive stability or an intra-cavity electro-optic modulator for fast path-length control [20]. However, both options come with technical challenges.

For the most advanced applications, not only the provision of a narrow-linewidth spectroscopy wave (idler), but also the determination of its absolute frequency ω_i is required. Therefore, a second approach to idler frequency stabilization appears better suited: *measure* the idler frequency and act *only* on the pump frequency to control the idler frequency (see Fig. 1(a)). This control works by exploiting the 1:1 transfer coefficient from pump frequency change to idler frequency change when the signal frequency is not acted upon, Eq. (1). The frequency of the signal wave is at all times determined by the optical length of the OPO cavity, following its variations due to perturbations. This is a source of frequency noise that needs to be compensated. The pump frequency will be regulated so as to keep the idler frequency precisely fixed at a desired value, compensating for both the OPO cavity length fluctuations as well as the pump laser's own fluctuations. Note that with this approach, neither the pump frequency nor the signal frequency will exhibit a particularly low frequency instability.

An example of this approach is the work of Peltola *et al.* [44]. They used second-harmonic generation (SHG) to bridge the gap between the idler frequency and the NIR, where the frequency of the second-harmonic (SH) wave $2\,\omega_i$ can be compared to mode of an OFC. In that work, the OFC was stabilized by locking the repetition rate to a hydrogen maser (H-maser) and the frequency $2\,\omega_i$ was determined using a frequency measurement of its beat with the OFC. A servo system acting on the pump frequency allowed obtaining a long-term stable idler wave frequency with Allan deviations at the sub-MHz level, but no reduction of its linewidth. The achieved frequency stability is summarized in Table 1.

Optics EXPRESS

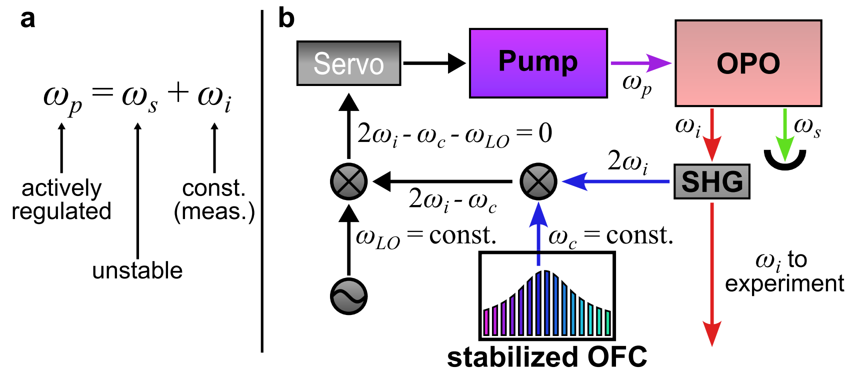

Fig. 1. Concept of the setup. a: The equation summarizes the concept. ω_p is regulated in order to keep the measured ω_i constant in time, while ω_s is left unstabilized and is affected by perturbations. **b:** An optically phase-locked OPO is implemented. The OPO is pumped at a frequency ω_p to generate the signal (ω_s) and idler (ω_i) frequencies. ω_i is then frequency-doubled in an SHG stage and mixed with an optically stabilized OFC, possessing a mode at frequency $\omega_c \approx 2\omega_i$. The generated beat is mixed with a local oscillator (LO) having a radio-frequency ω_{LO} in order to generate an error signal. It is the input to the servo that controls the pump frequency. Colored and black arrows are used for optical and analog signals, respectively. More details follow in Fig. 2.

In this work, we expand on this method, by implementing an ultrastable OFC and a phase-locked loop (PLL) of the idler frequency to this OFC, allowing to achieve not only long-term frequency stability but also excellent linewidth narrowing. The principle is shown in Fig. 1(b).

2. Experimental setup

Our apparatus consists of three main units, shown in Fig. 2. Unit 1 (top) comprises the OPO as well as the optical and electronic components of the locking subsystem. Unit 2 (center left) contains a first OFC (OFC1) and its reference laser (L1). These are used for the stabilization of the OPO's frequency. Unit 3 (bottom) serves to characterize the OPO in the locked state, and therefore includes a second OFC (OFC2) with its own reference laser (L2). Unit 4 (center right) provides the H-maser as a reference clock in the radio-frequency (RF) domain. It delivers ultrastable RF signals to the other three units and is also required for the optical frequency measurement. The H-maser is continuously compared to the national time standard PTB (Physikalisch-Technische Bundesanstalt, Braunschweig) via a common-view Global Navigation Satellite System (GNSS) technique. This ensures SI-traceability of the absolute frequencies. All units are computer-controlled and connected via a network. We now describe the units in more detail.

Unit 1 contains the actual OPO with its pump laser, a SHG stage to convert the idler radiation, a wavelength meter (High Finesse WS-7 IR Super Precision), locking and monitoring electronics. The OPO is a commercial system (TOPTICA DLC TOPO, [47]), that generates >1 W of output power over the idler wavelength range of 2.2 – 3.9 μm. The corresponding signal range is 1.45 – 2.07 μm. The system consists of the OPO laser head and a ytterbium-doped fiber amplifier (Yb-FA) with up to 10 W output power. To seed the amplifier, we employ a separate commercial semiconductor laser (1.06 μm, TOPTICA CTL 1050) to benefit from its narrower free-running linewidth (<10 kHz at 5 μs according to the manufacturer). When unstabilized, the linewidth of the OPO's idler was previously determined to be 1 – 2 MHz on a 25 ms timescale [47]. On similar timescales, but with the above seed laser, we observe a linewidth of $\simeq$ 100 kHz, which

Optics EXPRESS

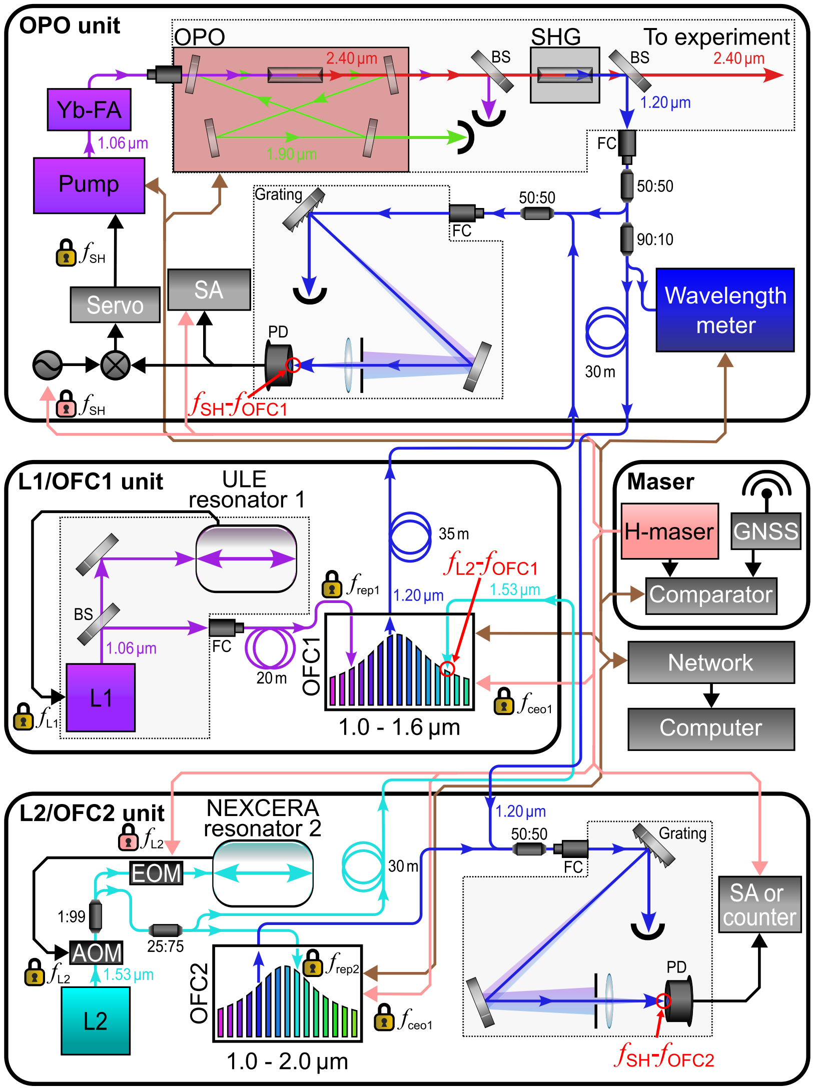

Fig. 2. Schematic of the setup. The individual black-framed boxes designate different units. **Top**: The OPO unit contains the OPO including pump and amplifier, the idler SHG unit and the wavelength meter, as well as the locking and monitoring electronics. **Center left**: The L1/OFC1 unit with the main reference laser L1, used to stabilize f_{rep1} of OFC1. A pick-off from OFC1 (shown here as an example centered at 1.2 μm) is sent to the OPO unit for idler frequency stabilization. **Bottom**: The L2/OFC2 unit, with L2 as the reference laser for f_{rep2} of OFC2. **Center right**: A hydrogen maser (H-maser) serves as the reference for all relevant RF sources. Individual wavelengths are shown in the figure by mapping the visible color spectrum to the wavelength range of the setup ([1.0 μm, 2.4 μm] → [purple, red]). Performance and measurements are monitored by computer control, connected to the individual components via network. Optical fibers are labeled for lengths >5 m. The H-maser analog signal, network connections, and other analog signals are shown in pink, brown, and black, respectively. Free-space parts of the setup are indicated as dashed-frame boxes. The padlocks symbolize active stabilization of the indicated frequency by a servo system (not shown). The padlock color gold denotes either a PLL lock or a PDH lock, while pink refers to a servo that implements a low-bandwidth frequency stabilization to the H-maser frequency. More details in the text. BS: beam splitter. FC: fiber coupler. AOM: acousto-optic modulator. EOM: electro-optic modulator. SA: spectrum analyzer.

increases to $3 - 5$ MHz on timescales of a few seconds, due to jitter. Typical frequency variations are 200 MHz over several hours, with drift rates on the order of 0.6 MHz/min.

The seed laser can be frequency-modulated with a high bandwidth (several ten MHz) via its current, which is crucial for realizing our locking scheme where the pump laser current is the actuator. Before being sent to the experiment, the full power of the OPO's idler wave is sent through a single-pass SHG setup containing a periodically poled lithium niobate crystal. In order to be able to generate the harmonic wave of the whole idler spectral range, we employ a crystal containing multiple grating periods, with periods between 33.3 μm and 36.0 μm, and operating temperature in the range $20 - 200\,^{\circ}$C. This combination of parameters allows us to find a suitable phase-matching condition for any wavelength in the idler's wavelength range. Owing to the high power of the idler radiation, a few milliwatts of the second-harmonic wave are generated in the single-pass configuration. This power is sufficiently high that the wave can be split into one part for generating a high-signal-to-noise-ratio beat with OFC1 and a second part for the wavelength meter, whose measurements are necessary for absolute frequency determination. To produce the beat, a fraction of the OFC1 output, spectrally centered around the idler's second-harmonic wavelength, is sent to the OPO unit via a 35 m long optical fiber, and there overlapped with the second-harmonic wave within the fiber, using a fiber combiner. The combined radiation is coupled out of the fiber, reflected off a grating, and directed onto the photodetector (PD). The signal-to-noise ratio of the beat generated in the PD is optimized by proper alignment of the grating. This beat signal is phase-locked to a RF signal of stable frequency (local oscillator, LO). To this end, the beat signal is mixed with the local oscillator (LO), and the low-frequency output of the mixer is the input to an appropriate servo that controls the pump laser's current, closing the loop. Overall, the idler frequency is phase-locked to a mode of the OFC.

Unit 2 contains the reference laser L1 (1.06 μm, Mephisto Innolight Nd:YAG) and OFC1 (Menlo Systems FC1500-250-ULN). Its repetition rate $f_{\mathrm{rep},1}$ is stabilized by phase-locking one comb mode to L1, while the carrier envelope offset frequency $f_{\mathrm{ceo},1}$ is stabilized to the H-maser. L1 itself is stabilized to a ULE resonator with a finesse of $\simeq 500\,000$ (resonator 1) using the Pound-Drever-Hall (PDH) technique, with the modulation applied to the laser's frequency actuator, a piezo-electric transducer.

Finally, in the lower part of Fig. 2, unit 3 contains the second OFC (OFC2) and a separate reference laser L2 at a wavelength of 1.53 μm (NKT Koheras Basik E15). Similar to above, the comb's repetition rate $f_{\mathrm{rep},2}$ is phase-locked to L2, while $f_{\mathrm{ceo},2}$ is stabilized to the H-maser. Except for the shared H-maser that provides f_{ceo} stabilization, the two combs are completely independent systems. L2 is also locked via the PDH technique to the resonator 2, a NEXCERA resonator [48] with a finesse of 700 000. NEXCERA is a novel spacer material for resonators [49], designed to be operated at room temperature. In contrast to L1, an acousto-optic modulator (AOM) is required for providing fast control of the frequency of the L2 output wave, since the laser itself does not have a high bandwidth modulation input. A sideband lock is implemented [50,51], where the laser wave is phase-modulated using an electro-optic modulator (EOM), and one of the modulation sidebands is locked to the resonator instead of the carrier. The sideband lock is used in order to be able to compensate the drift of the resonator. A detailed explanation is given in section 3.3. To characterize the performance of the two reference lasers, a portion of the radiation of L2 is sent to OFC1 and then measured against it.

3. Performance

In order to characterize the spectral properties of the OPO's idler radiation, beats between several sources were produced. In Fig. 2 these beats are indicated by red circles together with their corresponding optical frequency differences. First, a beat between OFC1 and L2, $f_{\mathrm{L2}} - f_{\mathrm{OFC1}}$, gives the combined instability level of the employed reference lasers L1, L2. Additionally, it

Optics EXPRESS

includes the locking performance of the PLL of OFC1 to L1 and any fiber noise originating from the 30 m long fiber used to send L2 radiation to OFC1.

In a second step, the PLL of the OPO is examined by monitoring the beat $f_{\mathrm{SH}} - f_{\mathrm{OFC1}}$ in the locked state. Finally, the absolute stability of the OPO's idler frequency is investigated, by measuring a beat between its SH wave and OFC2, $f_{\mathrm{SH}} - f_{\mathrm{OFC2}}$. This simultaneously gives the most accurate upper limit of the frequency instability for the system as a whole, including all fiber noise and other noises. The analysis for short timescales is presented in Section 3.1, and the analysis for long timescales follows in section 3.3. These analyses were performed with the OPO set to an idler wavelength of 2.81 μm, corresponding to a signal wavelength of 1.71 μm and an idler second-harmonic wavelength of 1.40 μm. In Sec. 3.5 we argue that the described performance can be achieved at all wavelengths within the output range of the OPO.

3.1. Short-term performance of the idler radiation

The beat $f_{\mathrm{L2}} - f_{\mathrm{OFC1}}$ shown in Fig. 3, panel 1a, is an average of many consecutive sweeps of the spectrum analyzer, each of duration 5 s and measured at a resolution bandwidth (RBW) of 1 Hz. Note that the individual traces could be averaged without any consideration of either resonator's drift, since the center frequency drifted by less than 1 Hz over the course of the entire data acquisition. This has two different reasons: in the case of resonator 1 the drift is negligible on the timescale of the measurement, and in the case of resonator 2 it is actively compensated, see sec. 3.3. From the beat we deduce a full-width half-maximum (FWHM) linewidth of 9 Hz. In the phase-noise spectrum of $f_{\mathrm{L2}} - f_{\mathrm{OFC1}}$, Fig. 3, panel 1b, small sidebands at frequencies of 50 Hz and 510 Hz can be observed. We believe that the origin is fiber noise occurring in both fibers that deliver the radiation from L1 and L2 to OFC1. Due to the modest strength of the sidebands, they are not significant for the current analysis and also have not impacted a recent spectroscopic study [25].

Data on the OPO's phase-locked loop performance, i.e. the frequency and phase noise of the beat $f_{\mathrm{SH}} - f_{\mathrm{OFC1}}$, is displayed in Fig. 3, center column. This data on the beat does not yet yield any information on the absolute stability of the idler frequency, but rather on how well it follows OFC1. The measured linewidth, 3 Hz FWHM, is caused by the RBW of the employed spectrum analyzer - as is expected for a properly working phase lock. From the phase-noise spectrum, panel 2b, we determine a signal-to-noise ratio of 70 dB in a RBW of 1 Hz. Additionally, a single significant sideband is observed, at a frequency of 810 Hz. The source for this is intrinsic to the setup: it is caused by acoustic noise originating from the Yb-FA, as was confirmed by a comparing the acoustic noise spectrum in the proximity of the OPO with the Yb-FA turned on and off.

Next, we consider the beat $f_{\mathrm{SH}} - f_{\mathrm{OFC2}}$. Its analysis is shown in Fig. 3, right column. Similar to panel 1a, panel 3a shows consecutive beat spectra measured over a total time of more than 30 min, averaged without any re-centering of individual traces. A Lorentzian fit finds a linewidth of 10 Hz (FWHM). This is only 1 Hz larger than the linewidth of the beat of the reference lasers (panel 1a). The spectrum (panel 1b) also exhibits several sidebands with frequencies in the range 10 - 50 Hz. These sidebands are not observed in the beats in panels 1a and 2a. The reason for this is that they are caused by fiber noise occurring in the 35 m long fiber guiding OFC1 radiation to the OPO (see Fig. 2), which only contributes to the measurements underlying panel 3, see section 3.2. In the phase-noise spectrum 3b, the sideband observed in the PLL signal at 810 Hz is again visible.

3.2. Fiber noise

To investigate the noise observed in the beat of the idler's second-harmonic and OFC2 (Fig. 3, panels 3a and 3b), the optical path between OFC1 and the OPO was investigated. To this end, a round-trip propagation path for the idler's second-harmonic was set up, by using two fibers similar

Optics EXPRESS

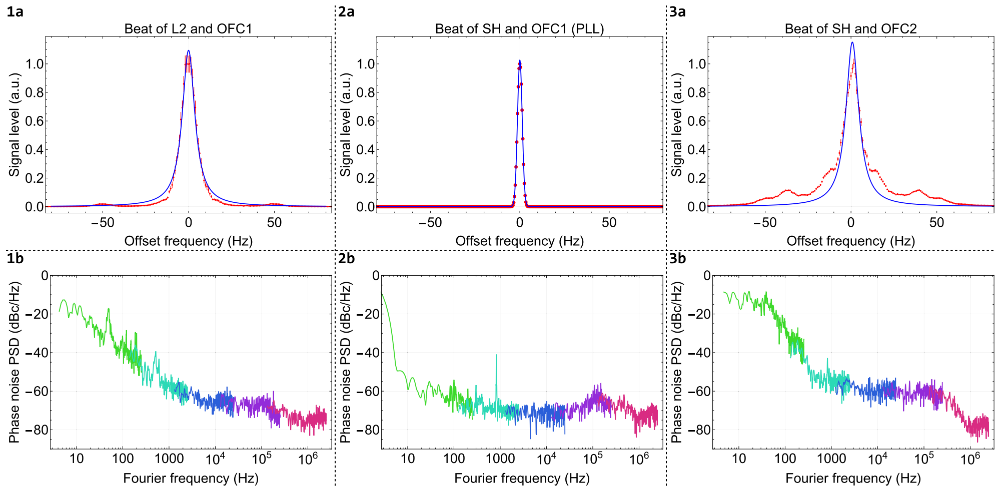

Fig. 3. Analysis of the beats between different units, marked by red circles in Fig. 2. Left column: beat $f_{L2} - f_{OFC1}$ between L2 and OFC1 locked to L1, showing the combined instability of the two reference lasers. **Center column** is the PLL of the OPO, specifically the beat between the second-harmonic of the idler and OFC1 in the phase-locked state, here at a second-harmonic wavelength of 1.4 μm. **Right column** shows the beat $f_{SH} - f_{OFC2}$ between the second-harmonic and OFC2, at the same wavelength 1.4 μm. This is a direct determination of an upper bound for the instability of the OPO's idler wave frequency and includes all noise sources of the system (e.g. noise of the lasers themselves and fiber noise). Each column is split into a determination of the linewidth of the beat (top) and the phase-noise power spectral density (bottom, PSD). For the linewidth plots of the first and last columns, the data are an average of many consecutive sweeps (order 10^2) of 5 s duration each, at 1 Hz RBW. The error bars are the standard error of the mean. The data are fit by a Lorentz function, giving a FWHM linewidth of 9 Hz and 10 Hz, respectively. For the middle column, the data is from a single spectrum analyzer sweep. It is fit by a Gauss function (FWHM 3 Hz), the appropriate form considering the digital band-pass of the spectrum analyzer.

to the one shown in Fig. 2 connecting OFC1 and OPO. The pick-off of the second-harmonic, previously sent to OFC2, is now sent to OFC1 and then back to the OPO. There, a self-beat is generated with a reference wave (the part that is usually sent to the wavelength meter). Additionally, sidebands are modulated onto the OPO's pump laser at 10 MHz, allowing a beat signal to be obtained at an RF frequency rather than at DC.

The result is shown in Fig. 4. As can be seen, multiple side-peaks are observed at different frequencies ranging from a few Hz to 80 Hz. This is not surprising, since the fiber is exposed to the environment and thus transfers acoustic and mechanical perturbations onto the light passing through it. Since the offset frequencies corresponding to the spectral peaks match well with the sideband frequencies observed in the beat between the idler's second-harmonic and OFC2, we infer that the sidebands are caused by this fiber noise. Additionally, a minor broadening of the carrier's linewidth is observed, 2 Hz. This can also explain the small broadening observed in the comparison of Fig. 3, panels 1a and 3a. We thus conclude that the fiber noise due to this fiber is the main source of frequency instability of the entire OPO metrology system, apart from the instability of the reference lasers themselves.

Optics EXPRESS

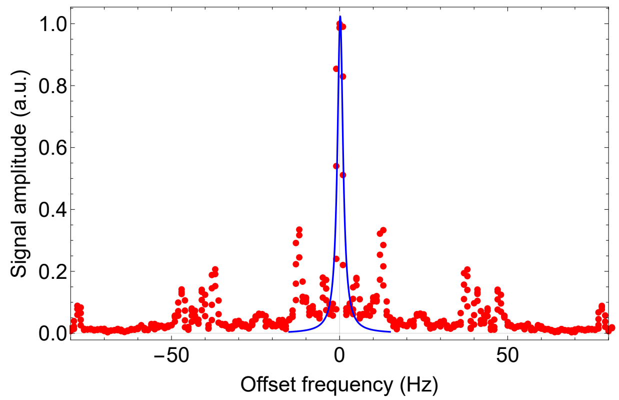

Fig. 4. Fiber noise of the longest fiber path in the system (35 m), connecting unit 1 and unit 2. The self-beat of the SH, sent on a round-trip to OFC1 and back, is shown in red. The blue curve is a Lorentzian fit to the central peak, yielding a FWHM linewidth of 2 Hz. The data was recorded using a spectrum analyzer with a sweep time of 200 s at a RBW of 1 Hz.

3.3. Compensation of the resonator drifts and frequency stability of the idler wave on long time intervals

As mentioned above, we actively compensate for both resonators' slow drifts. In the case of resonator 1, this is done in order to keep the idler frequency at a fixed absolute value, which is necessary for ultra-high precision spectroscopy. In the case of resonator 2, the OFC2 comb lines are kept at fixed values.

The drifts of resonator 1 and 2 are compensated independently and at a different stage of the optical setup. For laser L1, and consequently for OFC1, the resonator drift is not compensated. Instead, the LO frequency of the PLL of the idler to OFC1 is corrected; therefore, only the OPO's idler frequency will maintain a fixed absolute value. For resonator 2, the compensation is instead implemented via the EOM shown in the bottom unit in Fig. 2. Therefore, both the L2 output frequency (after the AOM) and the entire OFC2 are drift-compensated.

For both units, the compensation is implemented in a similar manner: the drift of each resonator is calculated from the absolute frequency value measured by each comb every 1 s relative to the H-maser. A moving average of the frequency data is computed and compared to a target frequency. The deviation of this average from the target is the error signal delivered to a digital PID loop that acts on the LO frequency or on the EOM frequency, respectively, for OPO and L2. Averaging times of 30 s for resonator 1 and 20 s for resonator 2 were found to lead to the best performance.

As a consequence of the two drift compensations, the idler frequency instability on long timescales shown in Fig. 5 (red) has to be interpreted in the following way. Since both of our combs measure the absolute frequency of the lasers relative to the H-maser frequency, the drift compensations described above effectively reference the idler's second-harmonic and the reference laser L2 (and thus also OFC2) to the H-maser. Since all RF devices used to record the shown data are also referenced to this H-maser, we are effectively measuring one maser-referenced frequency against another. Therefore, the instability averages down as the integration time increases.

Determining the absolute value of the optical frequency relative to the atomic unit of frequency (SI-traceability) requires that we continuously compare our H-maser frequency to a H-maser of PTB that is steered to the international atomic time. Our comparison occurs via common-view

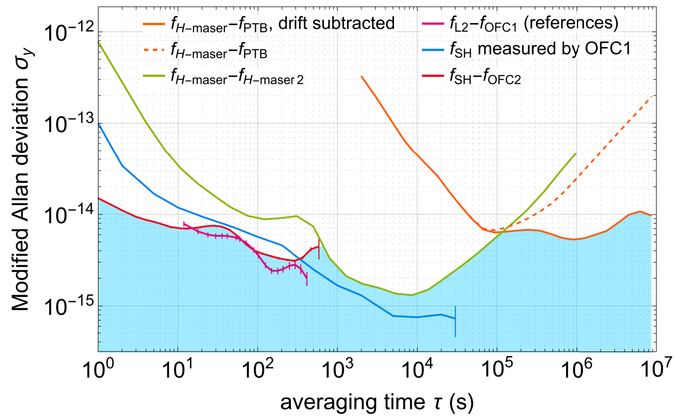

Fig. 5. Fractional Allan deviations of different signals. The magenta, blue and red traces show Allan deviations of an optical frequency. For magenta and red, the underlying data is the beat frequency between two waves, while for the blue trace it is the data calculated from Eq. (2), with f_{ceo1}, f_{rep1} and f_{beat1} measured simultaneously. All RF frequencies are either measured by a frequency counter or a spectrum analyzer, both of which are referenced to the H-maser. The green and orange traces show Allan deviations of the H-maser, evaluated by different methods. The upper limit of the blue shaded area depicts a conservative estimate of the fractional instability of the OPO's idler wave, inferred from the individual measurements. See text for explanations.

GNSS. The comparison determines the frequency offset of our H-maser's nominal 10 MHz signal and also the time drift of the offset. With this information, we can finally compute the lasers' absolute frequencies and their instabilities relative to the atomic frequency standard.

To demonstrate that our system is stabilized over long time intervals and to summarize the performance, we show in Fig. 5 six different fractional modified Allan deviations σ_y.

The dashed orange trace is the instability of the comparison of the frequency of our H-maser and the international atomic frequency standard at PTB. The upturn after approximately 1 day is due to the drift of the maser. The time-varying offset of our maser is recorded and taken into account in the OPO frequency data analysis in post-processing or in a feed-forward correction. The fractional drift rate is approximately 3×10^{-15} per day for this H-maser. The full orange line is obtained by removing the linear drift from the measured data and re-evaluating the Allan deviation. Since the GNSS receiver provides one reading every 15 min, no Allan deviation can be determined for short integration times.

The green trace is the Allan deviation of a comparison of the H-maser with a similar device, recorded at a different time. The Allan deviation reflects the combined instability of the two masers. Since both are nominally equal, the instability of the maser used in the OPO stabilization is expected to be slightly less than the values of the trace. This trace extends to integration times shorter than 15 min. The low instability verified on such shorter timescales is an important feature, since the drift compensation described above relies on locking the lasers' frequencies to the maser with time constants on the order of $10^1 - 10^2$ s.

The magenta trace shows the Allan deviation of the drift-removed beat $f_{\text{L2}} - f_{\text{OFC1}}$. This is the relative instability of the two independent reference lasers. Note that OFC1 is not drift-compensated, so that similar to the maser data, a linear function was fitted to the raw beat data and subtracted from it, before computing the Allan deviation.

Finally, the red and blue traces refer to the Allan deviation of f_{SH}, and are obtained by two different methods. The first trace (blue) is the absolute frequency value f_{SH} determined by OFC1. This is achieved through the classic frequency comb equation for a to-be-determined optical frequency f_o

$$f_o = f_{ceo1} + nf_{rep1} + f_{beat1}, \tag{2}$$

where f_{ceo1} = 35.600 000 00(1) MHz for OFC1, n is the index of the comb mode used for locking and determined using the wavelength meter, and $f_{beat1} = f_{SH} - f_{OFC1}$ is the beat frequency between the SH of the idler and the closest mode of OFC1. Under phase-lock, f_{beat1} is equal to the local oscillator's frequency, typically in the range of 40 − 100 MHz. The repetition rate $f_{rep1} \simeq 250$ MHz is here measured once per second by a high-resolution frequency counter (Microsemi 3120A) referenced to the H-maser. The blue trace for f_{SH} averages down with increasing integration time. These Allan deviation values do not reflect the actual (absolute) instability of the idler frequency, but indicate that it is locked well to the OFC1 on the short time scale and to the H-maser on the long time scale.

The second trace for f_{SH} (red) is the normalized Allan deviation $\sigma_y(f_{SH} - f_{OFC2})$. Here, the data was recorded with another frequency counter, also with 1 s integration time. In this measurement, and for short averaging times, the Allan deviation results from the independent frequency fluctuations of the idler SH wave and the OFC2 comb mode. Thus, the plotted red values represent an upper bound for the instability of the idler SH wave. This bound is $\sigma_y(f_{SH}) \leq 1 \times 10^{-14}$ and applies also to the idler frequency itself. The red trace is not extended to longer integration times because it then no longer reflects the actual instability of the idler frequency. As explained, f_{SH} and f_{OFC2} are not independent on long timescales.

3.4. Absolute frequency comparison

The two employed combs OFC1, OFC2 may be used not only to characterize the instability of the system, but also to compare and verify that the same absolute frequency is measured by both combs and associated equipment. The task is accomplished by measurements similar to those presented in sections 3.1 and 3.3. Equation (2) is now applied to the two independent combs, and (f_{ceo}, f_{rep}) are measured by independent frequency counters, n is calibrated using a common wavelength meter, and the two beat frequencies f_{beat1}, f_{beat2} are measured with a spectrum analyzer and a frequency counter for OFC1 and OFC2, respectively. All counters and the spectrum analyzer are referenced to the common H-maser. Thus, in this characterization we focus on the optical metrology, and not on the performance of the RF reference. In a variation to the previous sections, the data in this context was taken for an idler SH wavelength of 1.20 μm. Additionally, a different reference laser L3 and ULE resonator, at 1.53 μm, were used to stabilize OFC1. We confirmed that the stabilized laser L3 had a similar level of frequency instability as the laser L1 used in the above sections, by characterizing it in a similar manner as is described for the comparison of L1 and L2 in sections 3.1 and 3.3.

The result is shown in Fig. 6. The data underlying the figure was taken simultaneously with the two combs and spans a duration of 2330 s. The raw f_{SH} data were averaged with different averaging times, and the mean of the averaged values is displayed in the figure. The statistical error associated with the points is the standard error of the means. The frequency counter used to count f_{rep} with OFC2 has a lower precision than the counter for OFC1, causing the larger statistical uncertainty, particularly apparent for small averaging times. The systematic uncertainty is given by the combined inaccuracy of the RF devices used in both measurements. The dominant contribution is from the spectrum analyzer used in the OFC1 measurement, which contributes 1.2 Hz uncertainty. All other contributions are on the order of a few millihertz or smaller. We found that for all averaging times, the two frequency values obtained with the two measurement systems based on OFC1 and OFC2 agree within the combined uncertainty. For the longest averaging time τ = 500 s, the difference between the two measured values is $\langle (f_{SH,OFC1})_\tau \rangle - \langle (f_{SH,OFC2})_\tau \rangle = (0.2 \pm 1.4)$ Hz, or $(0 \pm 6) \times 10^{-15}$ fractionally. Thus, 6×10^{-15} is a conservative estimate for the total fractional uncertainty of the idler frequency measurement

Optics EXPRESS

procedure by a single comb, excluding the uncertainty of the RF reference. (The latter is estimated to be at a similar level.)

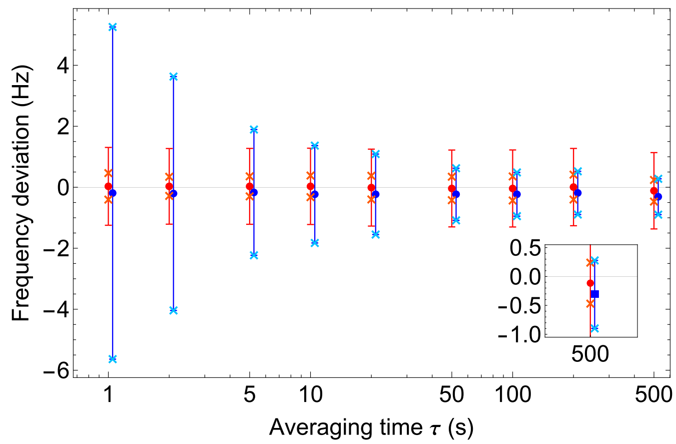

Fig. 6. The optical frequencies f_{SH} measured with OFC1 (red) and with OFC2 (blue), for different averaging times. The data are shown relative to an (arbitrary) offset frequency (approximately 249 THz). Two error bars are shown for each data set. The crosses represent the statistical standard error of the measurement, while the error bars denote the combination of statistical errors and systematic uncertainties. For clarity, the blue data points and errors are shown with a horizontal offset.

3.5. Stabilization of different idler wavelengths

As mentioned, the idler SHG sub-unit has been implemented in a way that it is capable of generating the second-harmonic wave over the entire tuning range of the idler. When changing the idler wavelength, it is necessary to change either the SHG crystal temperature, the grating period through which the laser wave propagates, or a combination of both. The crystal temperature is controlled by a commercial oven and an oven controller unit, obtained together with the crystal. We mounted the oven on a translation stage to allow for a fine adjustment of the crystal position perpendicular to the laser propagation direction. With this setup, a temperature change is possible within a few minutes, while a change of the grating period takes approximately thirty minutes due to the need for minor alignment optimization.

Therefore, the actual limiting factor of our method is the output range of the comb. For our OFC1, it is $1.0 - 1.6\ \mu$m, thus limiting the overall system's operation to the range $2.2 - 3.2\ \mu$m. Note that this could be extended by using OFC2 instead as the reference for the OPO, since it has a larger wavelength range than OFC1, reaching up to $2.0\ \mu$m. This potential exchange should not have a significant effect on the stability of the OPO, since both combs possess similar performance. For this reason, we believe that the full idler range of our OPO is lockable using our method.

We have phase-locked the OPO when tuned to the wavelengths 2.40, 2.60, 2.70, 2.81 μm, corresponding to 1.20, 1.30, 1.35, 1.40 μm for the SH. In all cases, we observed phase noise spectra and linewidths of the PLL similar to those shown in Fig. 3. These are provided as a supplemental document (see Supplement 1). We thus infer a similar level of idler frequency instability for these cases. For the specific cases of 2.40 μm and 2.60 μm, we have verified the performance by a beat with OFC2/L2, in the same way as was done for 2.80 μm, see sections 3.1 and 3.3. Therefore, we believe that our scheme will work well at any idler wavelength (even untested ones) and will provide similar frequency stability as the one presented above.

3.6. Long-term operation of the system

For providing long-term stability of the idler, we rely on the following procedure. After a thermalization of the setup, the range of the OPO's fast lock is sufficient to maintain the lock for a few hours. During operation, the SH frequency is measured by the wavelength meter, denoted f_{WM}. Due to an imperfect calibration of the wavelength meter, the value f_{WM} is offset from the correct value measured by the comb, by an amount $\Delta f_{\mathrm{WM}} = f_{\mathrm{WM}} - f_{\mathrm{SH,OFC1}}$, typically $10 - 30$ MHz. Therefore, while the OPO is in the locked state, Δf_{WM} is calibrated. When the OPO falls out of lock, f_{WM} will change. A digital control loop then pushes the frequency back to the calibrated offset, with feedback applied to the pump laser's piezo actuator. When the frequency is close to the lock point, the fast lock automatically re-engages, restoring the locked state. This procedure effectively re-centers the fast lock output and typically takes a few seconds.

We show in Fig. 7 f_{WM} over the course of a day. In the locked state, the idler accurately maintained the same target frequency, as confirmed by the continuous measurement with OFC1. Occasionally, wavelength jumps were detected by the wavelength meter. These are situations, where the OPO fell out of phase-lock and was quickly re-locked by the digital loop described above. The jumps are a result of the thermal drift of the OPO, which in our current setup is not compensated for by a slow lock, e.g. by controlling the piezo actuator of the pump laser.

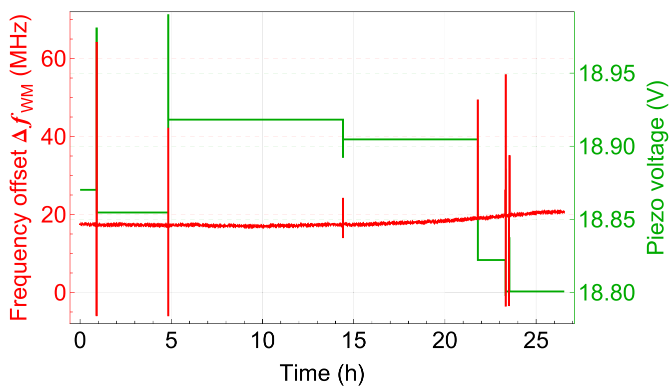

Fig. 7. Long-term stability of the system during of a typical measurement day. The red trace shows the wavelength of the idler's second harmonic measured by the wavelength meter (converted to frequency) relative to the value measured by OFC1. The nearly constant trace shows that the OPO was operating in the locked state nearly all the time. The offset ($\Delta f_{\mathrm{WM}} \simeq 18$ MHz) and its drift (3 MHz over 1 day) are systematic errors of the wavelength meter, consistent with its specifications. The green trace shows the voltage applied to the piezo actuator of the pump laser, which is used to re-lock the OPO. Jumps in the recorded wavelength meter reading correspond to instants when the OPO fell out of phase-lock and was subsequently automatically re-locked by changing the piezo actuator voltage. Typically, the out-of-lock periods lasted a few seconds.

The total unlocked time in Fig. 7 (67 s) relative to the measurement interval of 26 h corresponds to a duty cycle of 99.93 %. Importantly, we have operated the system in this configuration at multiple wavelengths daily over the course of more than two years, proving the stability and robustness of the setup. No major flaws or issues arose during this time.

4. Conclusion, application, and perspectives

We have developed an optical frequency metrology system based on an optical-parametric-oscillator. It exhibits a fractional frequency instability at the 1×10^{-14} level or smaller for integration times between 1 and 10^5 s and a linewidth of similar magnitude. Both of these

Optics EXPRESS

properties represent more than a hundredfold improvement over the previous state-of-the-art [20,45]. Our scheme was employed at several wavelengths within the idler range, proving the flexibility of the method. Additionally, the system has been operated long-term with a duty cycle above 99.9 %. The idler frequency is SI-traceable through a hydrogen-maser-referenced optical frequency comb that is continuously calibrated to the national standard via common-view GNSS. The total uncertainty of the idler frequency measurement relative to the RF reference is less than 6×10^{-15} and the RF frequency accuracy is approximately 1×10^{-14}, resulting in a total uncertainty of less than 1.2×10^{-14}. The system has been thoroughly analyzed and sources of noise have been identified. We find that the performance of the system is limited by the instability of the reference lasers and of the H-maser, as well as by fiber noise. In principle, these limits could be overcome by implementing a more stable reference laser [52,53], an optical fiber link to a national metrology laboratory [54–56], and active fiber noise cancellation [57], all of which have been demonstrated elsewhere.

In separate work, this system enabled the first Doppler-free spectroscopy of electric quadrupole vibrational transitions in a molecular ion, and furthermore permitted a SI-referenced measurement of their frequencies. Owing to the exceptional stability of the idler frequency, frequency scan step sizes as small as 5 Hz could be taken. This enabled measurements of spectroscopic lines with linewidths as small as $\simeq 6$ Hz, corresponding to line quality factors of up to 2.2×10^{13} [25,58]. This application example provides a separate confirmation of the results presented here. We have thus realized a powerful tool for mid-infrared precision spectroscopy, in particular when high power is required.

Based on the present work, we expect that the system can be expanded to alternatively stabilize the OPO's signal wave frequency (1.45 - 2.07 μm) to a similar stability level as shown here for the idler wave. Most of the wavelength range of the signal can be beaten directly with OFC2. A SHG unit is thus not required to bridge to the NIR regime, which simplifies the setup. However, the locking scheme employed here does not work for the signal wave, due to the OPO's cavity being resonant for the latter. Instead, we propose to implement a feedback control scheme using an AOM in the output path of the signal wave, which will act as a fast frequency shifter. A down-stream beat with the OFC would enable both the generation of an error signal for a PLL with feedback applied to the AOM as well as an absolute frequency measurement. Note that long-term stability requires the absence of mode-hops. The mode-hop free tuning range of the signal radiation is on the order of 10^2 MHz, which is similar in magnitude to its drift over a few hours (inferred from the observation of the idler drift, see Sec. 2). Therefore, we expect that long-term stability can be achieved by incorporating a slow servo that controls the OPO cavity length. Note that in this case, the idler locking scheme does not need to be operated and that the pump and idler radiations remain unaffected since the AOM frequency shift is applied once the signal radiation has left the OPO. With such a scheme, it should be possible to extend the output spectral range of the metrology system to include 1.45 - 2.07 μm.

Longer wavelengths than those presented in this work should also be realizable as an extension of our setup, as follows. With the use of an additional laser source in the NIR range, e.g. an amplified fiber laser at 1.5 μm, phase-locked to the same OFC, and a suitable crystal that allows for difference-frequency generation (DFG), the generation of cw radiation up to $\simeq 8$ μm is straightforward [59,60]. The 1.5 μm radiation can be mixed with either the frequency-stable idler wave or the frequency-stable signal wave, resulting in far-IR radiation with frequency stability expected to be similar to that presented here for the idler.

Funding. Heinrich-Heine-Universität Düsseldorf; Deutsche Forschungsgemeinschaft (INST-208/774-1 FUGG, INST-208/796-1 FUGG); H2020 European Research Council (786306, "PREMOL"); European Partnership on Metrology (23FUN04 COMOMET).

Acknowledgments. The assistance of U. Rosowski in the maintenance of the H-maser and with concomitant data analysis has been important and is much appreciated. C. Wellers contributed in conceptual analyses and in procuring the OPO. M. G. Hansen and I. V. Kortunov are also acknowledged for their contributions to procurement of the OPO and for

Optics EXPRESS

their help during set up of the OPO's and comb's infrastructure. We thank E. Wiens for the provision of L3. C. J. Kwong assisted in the maintenance of OFC2. The performance of the system was validated in high-resolution spectroscopy in joint work with S. Alighanbari.

Disclosures. The authors declare no conflicts of interest.

Data availability. Data underlying the results presented in this paper are not publicly available at this time but may be obtained from the authors upon reasonable request.

Supplemental document. See Supplement 1 for supporting content.

References

1. S. T. Yang, R. C. Eckardt, and R. L. Byer, "Continuous-wave singly resonant optical parametric oscillator pumped by a single-frequency resonantly doubled Nd:YAG laser," Opt. Lett. **18**(12), 971–973 (1993).
2. W. R. Bosenberg, A. Drobshoff, J. I. Alexander, *et al.*, "93% pump depletion, 3.5-W continuous-wave, singly resonant optical parametric oscillator," Opt. Lett. **21**(17), 1336–1338 (1996).
3. K. Schneider, P. Kramper, S. Schiller, *et al.*, "Toward an optical synthesizer: a single-frequency parametric oscillator using periodically poled $LiNbO_3$," Opt. Lett. **22**(17), 1293–1295 (1997).
4. S. Schiller and J. Mlynek, "Continuous-wave optical parametric oscillators," Appl. Phys. B **66**(6), 661–764 (1998). Special Issue, Editors: S. Schiller, J. Mlynek.
5. D. J. M. Stothard, M. Ebrahimzadeh, and M. H. Dunn, "Low-pump-threshold continuous-wave singly resonant optical parametric oscillator," Opt. Lett. **23**(24), 1895–1897 (1998).
6. M. H. Dunn and M. Ebrahimzadeh, "Parametric Generation of Tunable Light from Continuous-Wave to Femtosecond Pulses," Science **286**(5444), 1513–1517 (1999).
7. D. Weise, U. Strößner, A. Peters, *et al.*, "Continuous-wave 532-nm-pumped singly resonant optical parametric oscillator with periodically poled $KTiOPO_4$," Opt. Commun. **184**(1-4), 329–333 (2000).
8. T. Petelski, R. S. Conroy, K. Bencheikh, *et al.*, "All-solid-state, tunable, single-frequency source of yellow light for high-resolution spectroscopy," Opt. Lett. **26**(13), 1013–1015 (2001).
9. E. V. Kovalchuk, D. Dekorsy, A. I. Lvovsky, *et al.*, "High-resolution Doppler-free molecular spectroscopy with a continuous-wave optical parametric oscillator," Opt. Lett. **26**(18), 1430–1432 (2001).
10. A. Hecker, M. Havenith, C. Braxmaier, *et al.*, "High resolution Doppler-free spectroscopy of molecular iodine using a continuous wave optical parametric oscillator," Opt. Commun. **218**(1-3), 131–134 (2003).
11. D. D. Arslanov, S. M. Cristescu, and F. J. M. Harren, "Optical parametric oscillator based off-axis integrated cavity output spectroscopy for rapid chemical sensing," Opt. Lett. **35**(19), 3300–3302 (2010).
12. M. Vainio, M. Merimaa, and L. Halonen, "Frequency-comb-referenced molecular spectroscopy in the mid-infrared region," Opt. Lett. **36**(21), 4122–4124 (2011).
13. S. Thorwirth, J. Krieg, V. Lutter, *et al.*, "High-resolution OPO spectroscopy of Si_2C_3 at 5μm: Observation of hot band transitions associated with ν_3," J. Mol. Spectrosc. **270**(1), 75–78 (2011).
14. I. Ricciardi, E. D. Tommasi, P. Maddaloni, *et al.*, "Frequency-comb-referenced singly-resonant OPO for sub-Doppler spectroscopy," Opt. Express **20**(8), 9178–9186 (2012).
15. D. Zhao, K. D. Doney, and H. Linnartz, "High-resolution infrared spectra of vibrationally excited HC_4H in a supersonic hydrocarbon plasma jet," J. Mol. Spectrosc. **296**, 1–8 (2014).
16. H. Chadwick, P. M. Hundt, M. van Reijzen, *et al.*, "Quantum state specific reactant preparation in a molecular beam by rapid adiabatic passage," J. Chem. Phys. **140**(3), 034321 (2014).
17. M. Vainio and L. Halonen, "Mid-infrared optical parametric oscillators and frequency combs for molecular spectroscopy," Phys. Chem. Chem. Phys. **18**(6), 4266–4294 (2016).
18. C. R. Markus, S. Thorwirth, O. Asvany, *et al.*, "High-resolution double resonance action spectroscopy in ion traps: vibrational and rotational fingerprints of $CH_2NH_2^+$," Phys. Chem. Chem. Phys. **21**(48), 26406–26412 (2019).
19. C. R. Markus and B. J. McCall, "Highly accurate experimentally determined energy levels of H_3^+," J. Chemical Phys. **150**(21), 214303 (2019).
20. Z.-T. Zhang, C.-F. Cheng, Y. R. Sun, *et al.*, "Cavity ring-down spectroscopy based on a comb-locked optical parametric oscillator source," Opt. Express **28**(19), 27600–27607 (2020).
21. D. Gupta, W. G. D. P. Silva, J. L. Doménech, *et al.*, "High-resolution rovibrational and rotational spectroscopy of the singly deuterated cyclopropenyl cation, c-$C_3H_2D^+$," Faraday Discuss. **245**, 298–308 (2023).
22. C. Wunderlich and C. Balzer, "Quantum measurements and new concepts for experiments with trapped ions," in *Advances in Atomic, Molecular, and Optical Physics* Vol. 49, (Academic Press, 2003), pp. 295–376.
23. S. Schiller, "Hydrogenlike Highly Charged Ions for Tests of the Time Independence of Fundamental Constants," Phys. Rev. Lett. **98**(18), 180801 (2007).
24. E. G. Myers, "CPT tests with the antihydrogen molecular ion," Phys. Rev. A **98**(1), 010101 (2018).
25. M. R. Schenkel, S. Alighanbari, and S. Schiller, "Laser spectroscopy of a rovibrational transition in the molecular hydrogen ion H_2^+," Nat. Phys. **20**(3), 383–388 (2024).
26. M. Niu, E. Salumbides, G. Dickenson, *et al.*, "Precision spectroscopy of the $X^1\Sigma_g^+, \nu = 0 \rightarrow 1 (J = 0 - 2)$ rovibrational splittings in H_2, HD and D_2," J. Mol. Spectrosc. **300**, 44–54 (2014).
27. A. Fast and S. A. Meek, "Sub-ppb Measurement of a Fundamental Band Rovibrational Transition in HD," Phys. Rev. Lett. **125**(2), 023001 (2020).

Optics EXPRESS

28. A. Fast and S. A. Meek, "Precise measurement of the D_2 $S_1(0)$ vibrational transition frequency," Mol. Phys. **120**(19-20), e1999520 (2022).
29. H. Fleurbaey, A. O. Koroleva, S. Kassi, *et al.*, "The high-accuracy spectroscopy of H_2 rovibrational transitions in the (2-0) band near 1.2 μm," Phys. Chem. Chem. Phys. **25**(21), 14749–14756 (2023).
30. J. Komasa, "Energy levels of the hydrogen molecule from relativistic nonadiabatic calculations," in *International Conference on Precision Physics and Fundamental Physical Constants (FFK)*, (Vienna, Austria, 2023).
31. Q.-H. Liu, Y. Tan, C.-F. Cheng, *et al.*, "Precision spectroscopy of molecular hydrogen," Phys. Chem. Chem. Phys. **25**(41), 27914–27925 (2023).
32. K. Pachucki and J. Komasa, "Rovibrational levels of helium hydride ion," J. Chemical Phys. **137**(20), 204314 (2012).
33. M. Kajita and N. Kimura, "Prospect for Vibrational Transition Frequency Measurement of Rare-gas Hydride Ions," J. Phys. Soc. Jpn. **89**(11), 114301 (2020).
34. S. Schiller, D. Bakalov, and V. I. Korobov, "Simplest molecules as candidates for precise optical clocks," Phys. Rev. Lett. **113**(2), 023004 (2014).
35. J.-P. Karr, "H_2^+ and HD^+: candidates for a molecular clock," J. Mol. Spectrosc. **300**, 37–43 (2014).
36. M. Kajita, G. Gopakumar, M. Abe, *et al.*, "Test of m_p/m_e changes using vibrational transitions in N_2^+," Phys. Rev. A **89**(3), 032509 (2014).
37. F. Wolf, J. C. Heip, M. J. Zawierucha, *et al.*, "Prospect for precision quantum logic spectroscopy of vibrational overtone transitions in molecular oxygen ions," New J. Phys. **26**(1), 013028 (2024).
38. S. A. Diddams, D. J. Jones, L.-S. Ma, *et al.*, "Optical frequency measurement across a 104-THz gap with a femtosecond laser frequency comb," Opt. Lett. **25**(3), 186–188 (2000).
39. R. Holzwarth, T. Udem, T. W. Hänsch, *et al.*, "Optical Frequency Synthesizer for Precision Spectroscopy," Phys. Rev. Lett. **85**(11), 2264–2267 (2000).
40. H. Inaba, T. Ikegami, F.-L. Hong, *et al.*, "Phase locking of a continuous-wave optical parametric oscillator to an optical frequency comb for optical frequency synthesis," IEEE J. Quantum Electron. **40**(7), 929–936 (2004).
41. E. V. Kovalchuk, T. Schuldt, and A. Peters, "Combination of a continuous-wave optical parametric oscillator and a femtosecond frequency comb for optical frequency metrology," Opt. Lett. **30**(23), 3141–3143 (2005).
42. N. Poli, C. W. Oates, P. Gill, *et al.*, "Optical atomic clocks," Rivista del Nuovo Cimento **36**, 555 (2013).
43. A. D. Ludlow, M. M. Boyd, J. Ye, *et al.*, "Optical atomic clocks," Rev. Mod. Phys. **87**(2), 637–701 (2015).
44. J. Peltola, M. Vainio, T. Fordell, *et al.*, "Frequency-comb-referenced mid-infrared source for high-precision spectroscopy," Opt. Express **22**(26), 32429–32439 (2014).
45. I. Ricciardi, S. Mosca, M. Parisi, *et al.*, "Sub-kilohertz linewidth narrowing of a mid-infrared optical parametric oscillator idler frequency by direct cavity stabilization," Opt. Lett. **40**(20), 4743–4746 (2015).
46. J. Karhu, M. Vainio, M. Metsälä, *et al.*, "Frequency comb assisted two-photon vibrational spectroscopy," Opt. Express **25**(5), 4688–4699 (2017).
47. D. B. Foote, M. J. Cich, W. C. Hurlbut, *et al.*, "High-resolution, broadly-tunable mid-IR spectroscopy using a continuous wave optical parametric oscillator," Opt. Express **29**(4), 5295–5303 (2021).
48. C. J. Kwong, M. G. Hansen, J. Sugawara, *et al.*, "Characterization of the long-term dimensional stability of a NEXCERA block using the optical resonator technique," Meas. Sci. Technol. **29**(7), 075011 (2018).
49. I. Ito, A. Silva, T. Nakamura, *et al.*, "Stable CW laser based on low thermal expansion ceramic cavity with 4.9 mHz/s frequency drift," Opt. Express **25**(21), 26020–26028 (2017).
50. J. I. Thorpe, K. Numata, and J. Livas, "Laser frequency stabilization and control through offset sideband locking to optical cavities," Opt. Express **16**(20), 15980–15990 (2008).
51. A. Y. Nevsky, S. Alighanbari, Q. Chen, *et al.*, "Robust frequency stabilization of multiple spectroscopy lasers with large and tunable offset frequencies," Opt. Lett. **38**(22), 4903 (2013).
52. S. Häfner, S. Falke, C. Grebing, *et al.*, "8×10^{-17} fractional laser frequency instability with a long room-temperature cavity," Opt. Lett. **40**(9), 2112–2115 (2015).
53. A. Didier, S. Ignatovich, E. Benkler, *et al.*, "946-nm Nd:YAG digital-locked laser at $1.1{\times}10^{-16}$ in 1 s and transfer-locked to a cryogenic silicon cavity," Opt. Lett. **44**(7), 1781–1784 (2019).
54. K. Predehl, G. Grosche, S. M. F. Raupach, *et al.*, "A 920-kilometer optical fiber link for frequency metrology at the 19th decimal place," Science **336**(6080), 441–444 (2012).
55. D. Husmann, L.-G. Bernier, M. Bertrand, *et al.*, "SI-traceable frequency dissemination at 1572.06 nm in a stabilized fiber network with ring topology," Opt. Express **29**(16), 24592–24605 (2021).
56. C. Clivati, M. Pizzocaro, E. Bertacco, *et al.*, "Coherent Optical-Fiber Link Across Italy and France," Phys. Rev. Appl. **18**(5), 054009 (2022).
57. L.-S. Ma, P. Jungner, J. Ye, *et al.*, "Delivering the same optical frequency at two places: accurate cancellation of phase noise introduced by an optical fiber or other time-varying path," Opt. Lett. **19**(21), 1777–1779 (1994).
58. S. Alighanbari, M. R. Schenkel, S. Schiller, *et al.*, subm.
59. S. Vasilyev, S. Schiller, A. Nevsky, *et al.*, "Broadly tunable single-frequency cw mid-infrared source with milliwatt-level output based on difference-frequency generation in orientation-patterned GaAs," Opt. Lett. **33**(13), 1413–1415 (2008).
60. K. Devi, P. G. Schunemann, and M. Ebrahim-Zadeh, "Continuous-wave, multimilliwatt, mid-infrared source tunable across 6.4-7.5μm based on orientation-patterned GaAs," Opt. Lett. **39**(23), 6751–6754 (2014).